Construction and Building Materials 257 (2020) 119552

Contents lists available at ScienceDirect

Construction and Building Materials

journal homepage: www.elsevier.com/locate/conbuildmat

Environmentally benign production of one-part alkali-activated slag with calcined oyster shell as an activator

Beomjoo Yang [a], Jeong Gook Jang [b,*]

[a] School of Civil Engineering, Chungbuk National University, Chungdae-ro 1, Seowon-gu, Cheongju, Chungbuk 28644, Republic of Korea
[b] Division of Architecture and Urban Design, Institute of Urban Science, Incheon National University, 119 Academy-ro, Yeonsu-gu, Incheon 22012, Republic of Korea

HIGHLIGHTS

- Oyster shell waste was calcined to produce an environmentally friendly and economical solid activator.
- Production of one-part alkali-activated slag with calcined oyster shell was extensively studied.
- Improved mechanical properties and microstructural characteristics were observed.
- Calcined oyster shell powder at excessive dosages induced a negative effect.

ARTICLE INFO

Article history:
Received 20 May 2019
Received in revised form 6 April 2020
Accepted 12 May 2020

Keywords:
One-part alkali activated-materials
Alkali-activated slag
Activator
Shell waste
Microstructure

ABSTRACT

This study focuses on an environmental friendly, non-corrosive and non-viscous activator during the production of one-part alkali-activated slag using calcined oyster shell (COS) powder. Test results demonstrate improved mechanical and microstructural characteristics for specimens prepared with COS powder as an activator. The highest increment in the strengths was revealed with a 5% COS addition due to the resulting enhanced pore refinement, whereas an excessive dose resulted in a delayed rate of C-S-H formation and a significant amount of large capillary pores, thus decreasing the strength. The mineralogical and microstructural properties of the paste were also analyzed, and these findings revealed that COS powder is suitable for use as an activator to produce one-part alkali-activated materials.

1. Introduction

In the face of carbon dioxide emissions and the depletion of natural resources associated with the production of Portland cement, studies of alternative low-CO_2 cement-based materials that are environmentally friendly and low in CO_2 emissions are recently gaining attention [1,2]. Alkali-activated materials are attractive and promising materials in this respect [3]. A typical difference in alkali-activated materials compared to Portland cement is the use of industrial byproducts or clay materials with alkali activation in manufacturing, and the engineering properties of alkali-activated materials are comparable to those of Portland cement-based materials [4]. The history of studies on alkaline activation technology is not short, with many studies conducted in the last century. An archival description of alkali-activated materials can be found in several review studies [5–7]. In addition, materials design, reaction mechanisms, mechanical properties, workability and durability data, environmental assessments, barriers, and incentives of alkali-activated materials have been well documented in recently published articles [3].

Alkali-activated materials can be divided into two types depending on the skeletal molecular structure. Alkali-activated materials containing calcium-rich precursors, e.g., alkali-activated slag generally have Q^2 and $Q^2(1Al)$ structures with a lower coordination of Si, while alkali-activated materials containing low-calcium and aluminosilicate-rich precursors, e.g., alkali-activated fly ash (or geopolymer), have $Q^4(2Al)$ and $Q^4(3Al)$ structures with a higher coordination of Si [8]. In the former, the reaction takes place at room temperature, as in Portland cement, whereas the latter requires a slightly higher temperature for the polymerization reaction to take place. In this respect, the alkali-activated slag has long been used as a construction and building material in practice [5]. However, in spite of the numerous studies of alkali-activated materials conducted thus far, the use of alkali-activated materials in the construction industry is rare. Limitations of

* Corresponding author.
E-mail address: jangjg@inu.ac.kr (J.G. Jang).

https://doi.org/10.1016/j.conbuildmat.2020.119552
0950-0618/

alkali-activated materials have been discovered in several studies and include the following: 1) stability issues with the supply of raw materials such as industrial by-products and calcined clay, 2) the presence of carbon dioxide emissions from the production of alkaline activators, 3) difficulties in handling due to the corrosive and hazardous alkali activator, 4) issues related to the standardization and industrialization of the material, and 5) poor user perceptions of alkali-activated materials [5].

Conventional alkali-activated materials, on the other hand, generally consist of two components: a precursor and an alkali activator. The manufacturing process of two-part alkali-activated materials acts as a barrier to in situ applications because it deals with corrosive and hazardous alkali activators. In this context, recently, one-part alkali-activated materials, in which only water is mixed the dry mixture, are actively being studied [9]. One-part alkali-activated materials require a relatively small amount of a solid activator and are more economical, environmentally friendly, and user-friendly than the two-part system. Differences in materials design of one-part alkali-activated materials involve the precursor types and the solid activators. In the case of alkali-activated slag, anhydrous sodium metasilicate, sodium hydroxide, and sodium carbonate have been studied as alkali activators [9–18]. However, sodium-based activators are relatively expensive to manufacture and have problems from a pragmatic viewpoint due to toxicity and a high pH [19]. On the other hand, Kim et al. investigated one-part alkali-activated slag using calcium oxide as a solid activator and reported that the material is cost-competitive and has excellent mechanical strength [20].

The development of an economical activator which imposes only a low environmental burden compared to sodium hydroxide or sodium silicate has been prioritized in the research on alkali-activated materials [3]. On the other hand, oyster shell, a waste product generated in the fisheries sector that is composed of at least 90% calcium carbonate, is regarded as a type of limestone produced in the sea [21,22]. However, in many countries where oysters are consumed, oyster shells are often illegally dumped, buried, and fielded, where they become a social, environmental and/or health concern [23]. Many studies have attempted to find ways to recycle oyster shell, and utilization of oyster shell as a fine aggregates for concrete has been investigated [23]. Although the methods are not technically difficult and easily applicable, they are not technically valuable in terms of the effective utilization of waste as a resource. Nonetheless, oyster shell, which consists mostly of calcium carbonate, can be converted to calcium oxide through a calcination process [24]. If this material can be utilized as a solid activator, the environmentally benign production of a one-part alkali-activated material can be expected, with high environmental and economic value. Therefore, the present study investigated the production of one-part alkali-activated slag with calcined oyster shell as an activator given the need to develop one-part alkali-activated materials using more environmentally friendly and economical alkali activators. Oyster shell was calcined and pulverized and used as a solid activator. The oyster shell activator was mixed with slag to produce a dry mixture of one-part alkali-activated slag. The effects of the dosage of the calcined oyster shell activator on the physicochemical properties and mechanical performance of the one-part alkali-activated slag were then investigated.

2. Experimental procedure

2.1. Materials and specimen preparation

Ground-granulated blast furnace slag was used as a solid raw material here. The density, specific surface area and loss on ignition of the slag used in this study were 2.90 g/cm^3, 4220 cm^2/g and 0.20%, respectively. The chemical composition of the slag was analyzed by X-ray fluorescence (XRF) and is presented in Table 1. Oyster shell waste sourced from the south coast of South Korea was used to produce an environmentally friendly alkaline activator. Bulk oyster shells were scrubbed and washed to remove contaminants and salt and were then ground for the calcination step. The ground oyster shell was calcined in an electric furnace at a heating rate of 1 ℃/min at a maximum temperature of 1000 ℃ for 3 h. It was then powdered until it could pass a 150 μm sieve. The method used to prepare the calcined oyster shell powder can be found in a previous study conducted by the author [24]. The chemical composition and X-ray diffraction (XRD) pattern of the calcined oyster shell powder are presented in Table 1 and Fig. 1, respectively. Table 1 and Fig. 1 show that the calcined oyster shell powder is composed of 98% calcium oxide and has a crystal structure of lime.

A summarized flow chart of the production of the one-part alkali-activated slag with the calcined oyster shell powder is shown in Fig. 2. The calcined oyster shell powder was dry-mixed into the slag at 5, 10, 15 and 20% in terms of the weight of the dry mixture (slag + calcined oyster shell powder) before mixing with water. Alkali-activated slag paste specimens were prepared with a constant water-to-binder ratio of 0.4. The pastes were mixed for 5 min and were then cast into 50-mm-cubical molds. After casting, the specimens in the molds were sealed with plastic wrap to prevent the evaporation of water and were stored in a curing room at a controlled temperature of 20 °C for 24 h. They were then demolded and subsequently cured in water at 20 °C. Specimens with different dosages of the calcined oyster shell powder, i.e., 5, 10, 15 and 20%, were labelled as O5, O10, O15 and O20, respectively.

2.2. Test methods

The experimental programs were designed to determine the physical and chemical properties of the samples and to evaluate their mechanical performance capabilities. Isothermal conduction calorimetry, thermogravimetry (TG), Fourier transform infrared spectroscopy (FT-IR), XRD and mercury intrusion porosimetry (MIP) were conducted for the former objective, while compressive strength testing and measurements of the apparent density were conducted for the latter objective. The heat of hydration was measured using isothermal conduction calorimetry (TOKYO RIKO, Model MMC-511SV6) with an initial scanning rate of 30 s, a final recording rate of 300 s, a bath water temperature of 20 ℃, and a measuring time of 72 h. A TG analysis was conducted using TA Instruments SDT Q600 and DSC Q200 devices. The samples were heated to 1000 °C at a rate of 5 °C/min in a N_2 environment. The FT-IR analysis was conducted using a Bruker Vertex 80v instrument, with the spectra collected from 4000 to 400 cm^{-1}. XRD was conducted using a PANalytical 640c instrument by employing CuKα radiation at 40 kV and 30 mA, a scan speed of 0.2°/min and a

Table 1
Chemical compositions of blast furnace slag and calcined oyster shell powder measured by XRF.

wt%	CaO	Na_2O	MgO	Al_2O_3	SiO_2	P_2O_5	SO_3	Cl	K_2O	MnO	Fe_2O_3	SrO
Blast furnace slag	36.60	0.19	5.96	16.30	36.50	0.05	3.04	0.01	0.52	0.14	0.23	0.04
Calcined oyster shell powder	98.00	0.25	0.35	0.08	0.20	0.13	0.41	0.11	0.02	0.04	0.10	0.31

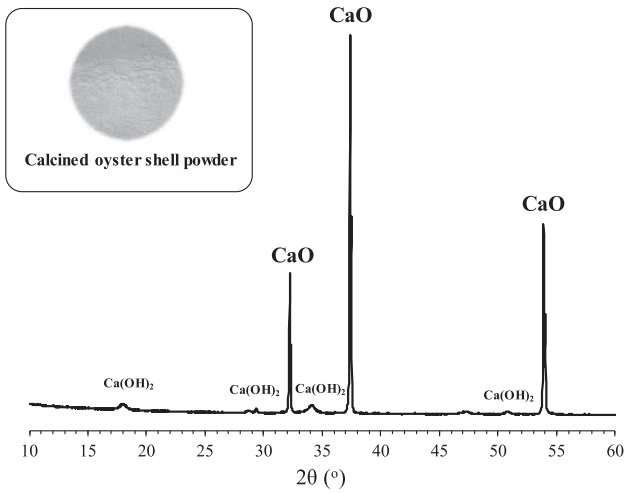

Fig. 1. XRD pattern of calcined oyster shell powder.

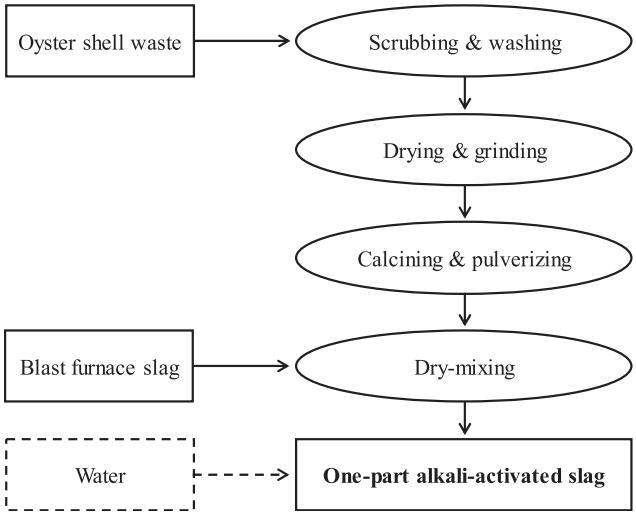

Fig. 2. A summarized flow chart of the production of the one-part alkali-activated slag with the calcined oyster shell powder.

scan range of 5–60°. The MIP test was conducted using an Autopore VI 9500 machine by Micromeritics Instrument Corporation with a pressure range of 0.1 to 60,000 psi. Water-cured samples at 28 days of age were used for the TG, FT-IR, XRD and MIP analyses. The compressive strength test utilized a compressive strength testing machine with a maximum loading capacity of 1000 kN. Three-day and 28-day specimens were used in the test, and the average compressive strength was calculated from three replicates.

3. Results and discussion

3.1. Mechanical properties

The effects of the calcined oyster shell activator on the compressive strength properties of the one part alkali-activated slag are shown in Fig. 3. It is evident from Fig. 3 that strength development is significantly affected by varying the dosages of the calcined oyster shell powder at later ages. The compressive strength outcomes for the specimens seeded with 5%, 10%, 15% and 20% of calcined oyster shell powder at three-days of age were 12.9 MPa, 13.9 MPa, 12.4 MPa and 11.4 MPa, respectively, thus showing similar strength values. However, at a later age (i.e., 28 days) the specimen seeded with 5% calcined oyster shell powder showed the highest compressive strength compared to the specimens containing calcined oyster shell powder at rates of 10%, 15% and 20%. Furthermore, with higher additions of the calcined oyster shell powder, i.e., greater than 5%, the compressive strength began to decrease. The recorded compressive strength values of the specimens seeded with 5%, 10%, 15% and 20% of calcined oyster shell powder at 28 days age were 35 MPa, 33.4 MPa, 27.2 MPa and 21.7 MPa, respectively.

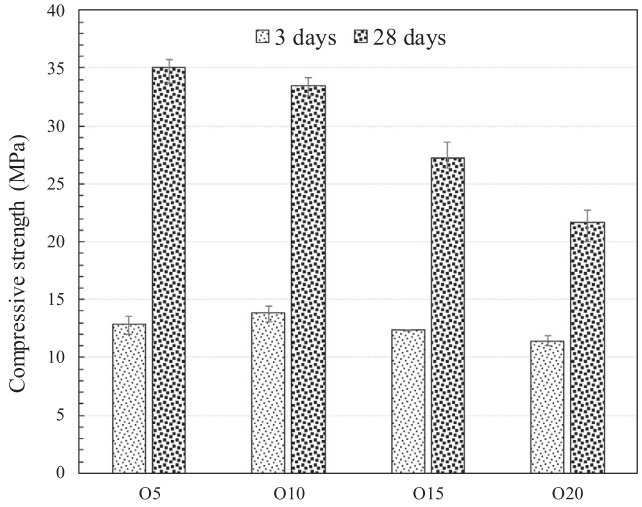

Fig. 3. Compressive strength of the one-part alkali-activated slag with calcined oyster shell activator.

The process of the reaction in alkali activate slag is a multistep mechanism which starts with the dissolution of Ca, Si and Al from the slag, progressing to re-orientation, then re-interaction, and then to condensation [25–27]. This process is a major factor defining the development of the strength of alkali-activated slag. Calcined oyster shell powder acts as an activator to break down the primary compounds to start the strength-forming reactions in alkali-activated slag. One possible reason for the negative effect of a higher dose (10–20%) on the strength development outcome is likely related to the un-reacted residue of the calcined oyster shell powder. Another factor affecting the strength loss can be the non-consumption of portlandite (owing to the high amount of CaO) to declassified C-S-H, which is the primary agent providing later-age strength development. Furthermore, it has been reported that the use of excessively high activator concentrations has a negative effect on the strength-gaining mechanism of alkali-activated slag [27]. Additionally, a high concentration of hydroxide ions can result in gel precipitation, which can hinder alkali activation at later stages, resulting in lower strength levels [28]. It should be noted that the use of calcined oyster shell powder excites the alkali activation potential of slag, as indicated by the strength-gaining phenomenon upon merely the addition of water (without any chemical agent).

3.2. Heat of hydration

The isothermal conduction calorimetry results of the one-part alkali-activated slag samples with varying dosages of the calcined oyster shell activator for the first 72 h of the reaction are shown in Fig. 4. Two distinctive peaks are observed at all dosages of the calcined oyster shell. Initial peaks appear after mixing with water, followed by accelerated peaks lasting from 12 to 26 h. Fig. 4a-A exhibits the first peak while Fig. 4a-B shows the second peak which

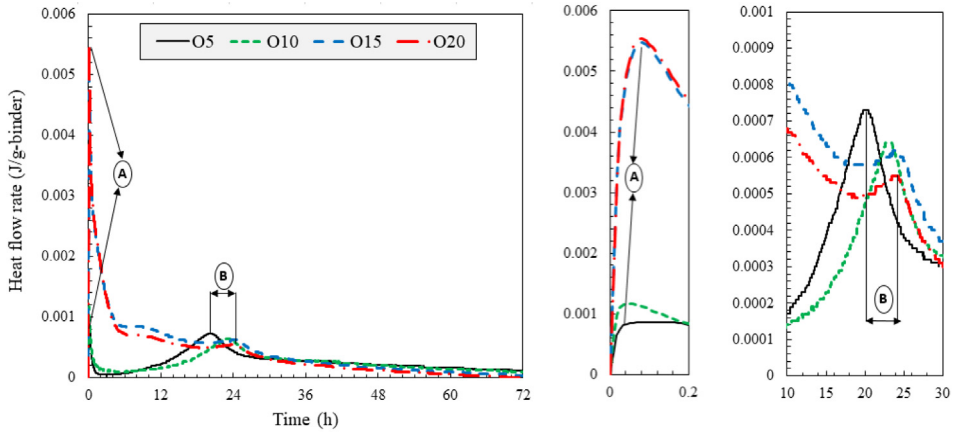

(a)

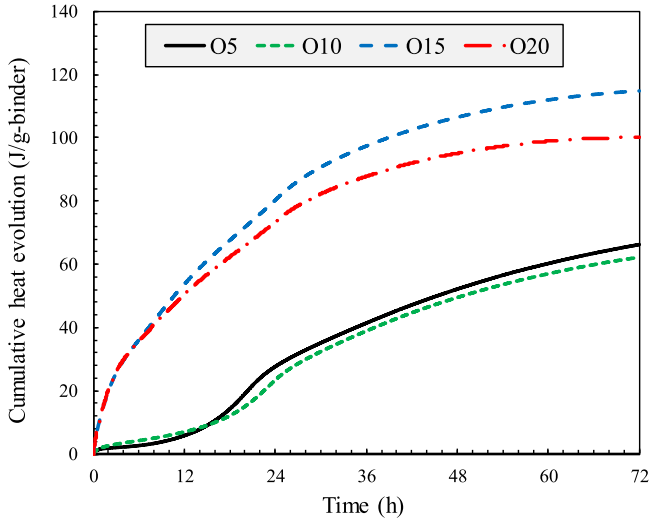

(b)

Fig. 4. Isothermal conduction calorimetry results of the one-part alkali-activated slag with calcined oyster shell activator: (a) heat flow rate and (b) cumulative heat evolution.

formed during the acceleratory period. The additional initial peak in the calcined oyster shell powder sample with the 5% dose during the pre-induction period (lasting from 8 to 10 h) is very diffuse, and no prominent accelerated hydration was noted. In contrast to the 5% and 10% additions, the samples seeded with 15% and 20% of calcined oyster shell powder exhibit a lower secondary peak. No additional peaks were observed beyond 26 h until the end of the test. Specimen seeding rates of 15% and 20% of calcined oyster shell powder led to increased heat evolution compared to the samples at lower dosages (i.e., 5% and 10%) as hydration continued. The highest peak was observed for the specimen seeded with oyster shell powder at 20%, while the lowest peak value was recorded for the specimen seeded at 5% of calcined oyster shell powder. However, an increase in the amount of calcined oyster shell powder leads to a delay in the second peak time and to lower peak values. The peak values were 0.00074 J/g at 20 h, 00064 J/g at 23 h, 0.00062 J/g at 23.5 h and 0.00054 J/g at 24 h for O5, O10, O15 and O20, respectively. These heat evolution curves resemble the type II hydration model of alkali-activated slag presented by Shi and Day, where two peaks appear, i.e., an initial peak before the induction period and a second hydration peak after the induction period [29]. The formation of both peaks is due to the dissolution of the calcium-rich calcined oyster shell powder; another cause is the contribution of the wetting and dissolution of ground-granulated blast furnace slag grains [15,29]. The cumulative heat evolution is significantly affected by specimen seeded with calcined oyster shell powder in amounts of 15% and 20% compared to the specimens seeded with calcined oyster shell powder in amounts of 5% and 10%, as shown in Fig. 4b. The formation of the second peak during the acceleratory period is generally altered by the rate of C-S-H phase formation [30]. These observations indicate that greater additions of calcined oyster shell powder in the slag affected the heat evolution peak time and peak value compared to specimens incorporating lower dosages of the calcined oyster shell powder. This can be attributed to the calcium-rich calcined oyster shell powder (CaO), which upon reacting with water may help to accelerate the reaction process of $Ca(OH)_2$. This may explain the development of high early age strength in the samples rich in calcined oyster shell powder. However, all samples with varying dosages showed nearly equal strength values during the early age test, confirming that higher dissolution heat of the calcined oyster shell powder is not the primary cause of the development of strength.

3.3. X-ray diffraction

Fig. 5 shows X-ray diffractograms of the raw slag and one-part alkali-activated slag with varying dosages of the calcined oyster shell activator. Peaks corresponding to calcite, a declassified product of C-S-H, are easily observable in all samples with varying dosages of the calcined oyster shell at 23-39° in 2θ, with the highest intensity appearing in the sample with a maximum dosage of calcined oyster shell powder of 20% at approximately 29-30° at 2θ. In addition, an earlier study of alkali-activated slag reported this high sharp peak as calcite, which is a residue of anhydrous slag [31]. However, the peak intensity decreased as the amount of calcined oyster shell dosages was reduced. Ettringite is present in all samples seeded with calcined oyster shell, forming when a sufficient amount of a calcium sulfate source is present. The intensity of ettringite is increased upon an increase in the dose of the calcined oyster shell powder. The presence of ettringite at this stage allows the classification of primary ettringite. This ettringite can slowly dissolve and reform at any voids or pores in the specimen after being exposed to water. At around 2θ = 18° and 34° at 28 days, sharp peaks of portlandite appeared. A higher intensity level of peaks appeared in samples incorporated with higher dosages of the calcined oyster shell powder. This can be regarded as the formation of portlandite from higher dosages of calcium oxide activator which were transformed into portlandite during the reaction with water. On the other hand, samples incorporated with 5% and 10% calcined oyster shell powder showed lower intensity levels, providing evidence of the effective consumption of portlandite to calcite. Portlandite, being soluble, can leach out from alkali-activated slag, leading to the formation of voids. It is important to note that the increment in the compressive strength in the specimen incorporating calcined oyster shell powder at a rate of 5% is influenced by the dual effect of pore refinement and the precipitation of calcite. Unconsumed portlandite in the specimens incorporated calcined oyster shell powder of rates of 10%, 15% and 20% exhibits a slower rate of the formation of calcite, leading lower compressive strength outcomes. Peaks of hydrotalcite and hydrotalcite-like phases were also recorded at 10–11.5° at 2θ in all samples. These compounds are some of the main reaction products in alkali-activated slag and are observable in the presence of a significant amount of Mg [32–35]. The formation of the hydrotalcite and hydrotalcite-like phases present some key trends. When the bulk Mg content is kept constant, a higher content of calcium promotes the formation of hydrotalcite phases during the alkali activation process. Consequently, it is probable that the amount of calcium available to react with Mg is significantly high, increasing the formation of crystalline hydrotalcite phases. Furthermore, these compounds have anion exchange properties and can displace calcium from portlandite and calcite, causing the strength to decrease. In raw slag, quartz was identified at 25° in 2θ. Upon alkali activation, the corresponding peak disappeared. This is the cause of the absence of a quartz peak in the calcined oyster shell powder alkali-activated slag. Furthermore, a peak associated with akermanite has been observed to exist at around 31-32° at 2θ in a crystalline form as unreacted raw slag according to the literature [33–37]. The presence of akermanite (Mg-based compound) likely stems from the formation of the hydrotalcite and hydrotalcite-like phases.

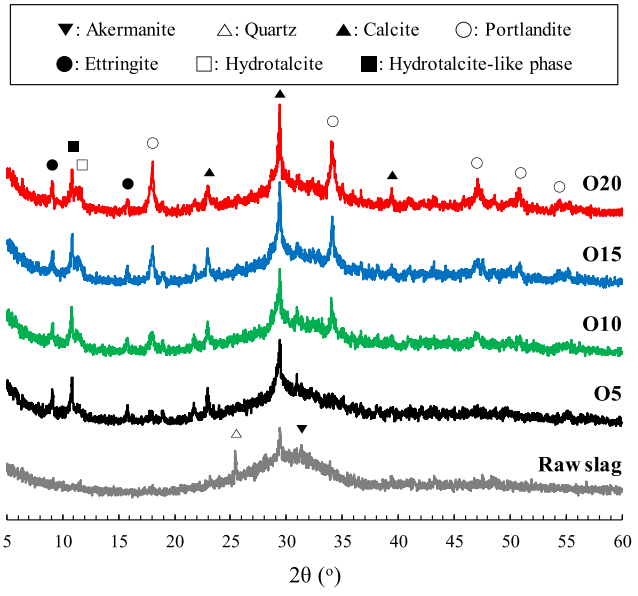

Fig. 5. XRD patterns for the raw slag and one-part alkali-activated slag with varying dosages of the calcined oyster shell activator.

3.4. Thermogravimetric analysis

The TG results of the one-part alkali-activated slag with the calcined oyster shell powder at dosages of 5%, 10%, 15% and 20% and cured at 28 days are shown in Fig. 6. Data interpretation of TG for the reaction product range is referenced from a previous study [20]. The weight losses in the TG data from 0 to 150 °C are an indicator of the decomposition of the main hydration products of cementitious materials, specifically C-S-H and AFt [38]. Fig. 6 implies that samples seeded with higher levels of calcined oyster shell powder receive more C-S-H than samples with lower dosages at 28 days of curing. The weight loss for the endothermic peak temperature range of 130–170 °C was attributed to the AFm phase [37]. Weight loss in the temperature range of 200–400 °C was attributed to the hydrotalcite and hydrotalcite-like phases [20]. Previous studies of synthetic hydrotalcite phases show two or more distinctive peaks in the temperature range of 250–400 °C [28,39]. However, no distinctive peaks have been observed for phases in alkali-activated slag on the TG curves despite the appearance of peaks in the XRD patterns [35]. These findings are in accordance with those in the present study. Samples incorporated with calcined oyster shell powder showed new peaks between 400 °C and 450 °C which were attributed to the decomposition temperature of calcium hydroxide [40]. Samples incorporated with calcined oyster shell powder at an amount of 20% showed significant weight loss at 430 °C compared to the other samples. The sample with lowest rate of the incorporation of oyster shell powder (i.e., 5%) showed very small or no weight loss at this point. Furthermore, all samples showed an inflection point in the temperature range of 600–700 °C, which is the decomposition range peak of calcium carbonate (calcite). Considering the C-S-H and hydrotalcite phases, it can be concluded that more C-S-H would form for the samples containing a high dosage of calcined oyster shell powder. However, the strength values are significantly different for different dosages of calcined oyster shell powder, indicating that the number of reaction products was not the governing factor for strength development.

3.5. Fourier transform infrared spectroscopy

Fig. 7 displays the FT-IR spectrum frequencies of the one-part alkali-activated slag with varying dosages of the calcined oyster shell powder. All samples show bands at 450, 530, 670, 874, 966, 1420, 1634, 3440 and 3643 cm^{-1}. The absorption at 450 cm^{-1} corresponds to the in-plane bending vibrations in the SiO_4 tetrahedra [8]. The bands at 669–707 cm^{-1} are related to symmetric stretching vibrations of Si-O-Si (Al) bridges [41]. All bands in the range of

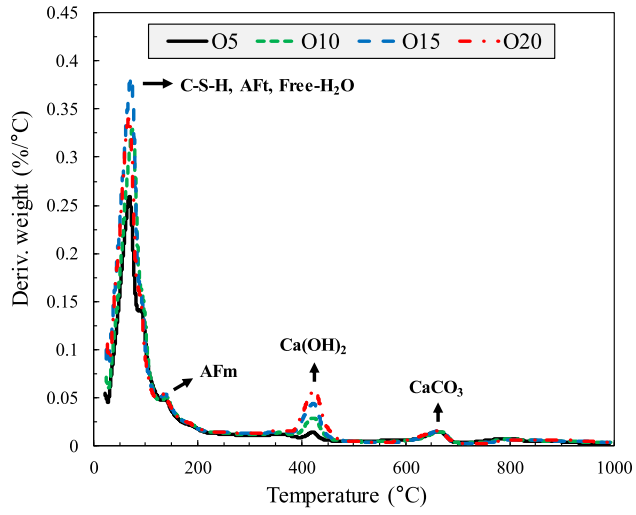

(a)

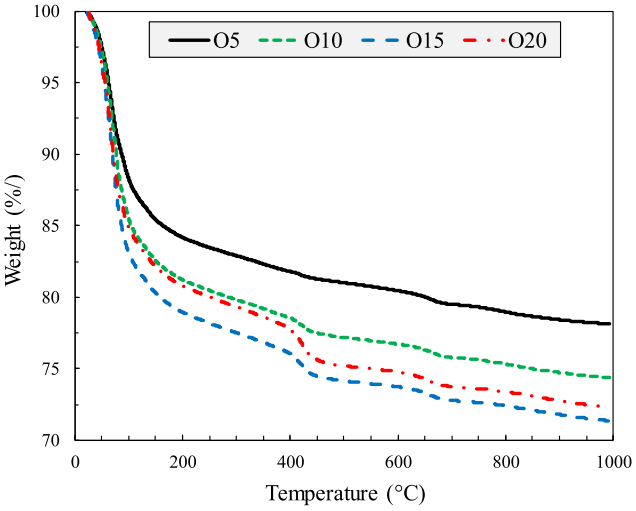

(b)

Fig. 6. TG results of the one-part alkali-activated slag with calcined oyster shell activator: (a) DSC curve and (b) TG curve.

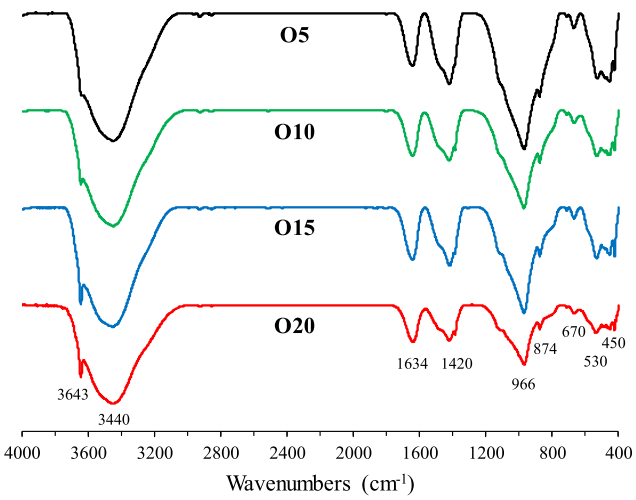

Fig. 7. FT-IR spectra of the one-part alkali-activated slag with calcined oyster shell activator.

800–1200 cm^{-1} correspond to the symmetric and asymmetric stretching of Si-O bonds [42]. A weak band at 874 cm^{-1} refers to the out-of-plane bending of CO_3^{2-}, while the presence of a large absorption band, i.e., a carbonate species in the range of 1400–1500 cm^{-1} stems from the asymmetric stretching vibrations (v_3) of CO_3^{2-} ions [42]. The specimens with higher dosages of the calcined oyster shell powder were less sensitive to atmospheric carbonation compared to those seeded with low dosages of the calcined oyster shell. The absorption at 966 cm^{-1} is due to the Si (Al)-O antisymmetric stretching vibration in the C-A-S-H gel. These bands refer to the presence of an orthosilicate unit with partial substitution of Si^{4+} by Al^{3+} in the tetrahedral position. This vibration band is sensitive to the C-A-S-H gel composition and depending on the ratio of Al/Si (increase or decrease), the vibration band shifts to a higher or lower wavenumber [43]. The band that originates at 1634 cm^{-1} and the broad band at 3440 cm^{-1} are associated with, respectively, the H–O–H bending vibration of molecular H_2O and the stretching vibrations of the OH groups in

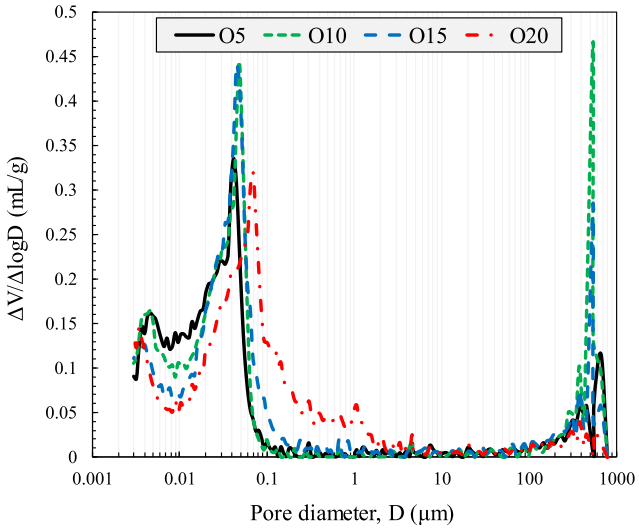

(a)

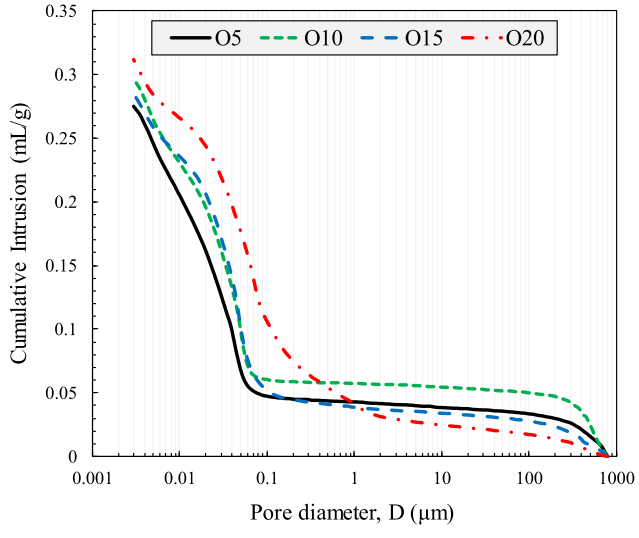

(b)

Fig. 8. MIP results of the one-part alkali-activated slag with calcined oyster shell activator: (a) pore size distribution and (b) cumulative intrusion of mercury.

Table 2
Microstructural characteristics of samples measured by MIP.

	O5	O10	O15	O20
Total pore area (m^2/g)	78.13	76.31	64.48	59.44
Median pore diameter (nm)	26.8	34.6	39.7	62.1
Average pore diameter (nm)	14.1	15.6	17.7	21.0
Apparent density (g/mL)	2.39	2.36	2.28	2.24

H_2O [8,42]. Peaks lacking sharp feature indicates wide SiQ^n(mAl) distributed units in their structures [8]. The narrow peak at 3643 cm^{-1} is related to the O–H stretching vibration of portlandite; the peak intensity decreased as the amount of calcined oyster shell powder is decreased [44]. It is evident from Fig. 8 that the calcined oyster shell samples with high doses have large absorption peaks, whereas the intensity decreases for those with low doses. These findings are in good agreement with the XRD results.

3.6. Mercury intrusion porosimetry

The pore size distribution of one-part alkali-activated slag samples incorporating calcined oyster shell powder at rates of 5%, 10%, 15% and 20% at 28 days are shown in Fig. 8. Two pore ranges are considered for the analysis of the pore size distribution of the samples. Pores 0.01–2 μm in size are considered to be capillary pores while pores between 100 and 1000 μm in sizes are entrained air bubbles [38]. Capillary pores greater than 0.05 μm reduce the strength while smaller pores less than 0.05 μm in size affect the shrinkage [38]. In this study, significant numbers of large capillary pores (0.05–1 μm) were observed for the samples incorporating higher dosages of the calcined oyster shell powder (i.e., O10, O15 and O20). On the other hand, the incorporation of 5% calcined oyster shell powder showed very few or no large capillary pores. Thus, the increased incorporation of the calcined oyster shell powder content did not effectively fill the capillary pores, and the presence of larger capillary pores is detrimental to the strength of the sample. This indicates that less calcined oyster shell powder led to relatively quicker pore-size refinement by filling the capillary pores and increasing the degree of microstructure densification compared to the other samples with higher levels of the calcined oyster shell powder. Table 2 also reflects a similar trend, showing lower median pore diameter values for the O5 sample compared to the O10, 015 and O20 samples. These observations are in good agreement with the compressive strength results, in which the incorporation of calcined oyster shell powder at a rate of 5% showed the highest compressive strength, with reduction in the strength when the amount of calcined oyster shell powder exceeded this level.

Furthermore, the samples with calcined oyster shell powder dosages of 5%, 10% and 15% showed numerous pores with diameters in the range of 100–1000 μm. These are most likely randomly incorporated air bubbles which arose during the sample preparation process, presumably caused by casting defects. However, these air bubbles have less influence on the strength compared to capillary pores due to their spherical shape.

4. Conclusions

This study investigated the effect of calcined oyster shell powder as a potential activator for the production of one-part alkali-activated slag. The calcined oyster shell powder was dry-mixed into slag at 5, 10, 15 and 20% by weight of the dry mixture (slag + calcined oyster shell powder). Conclusions based on the compressive strength, isothermal conduction calorimetry, XRD, TG, FT-IR and MIP analyses are presented below.

1) During the hydration process of one-part alkali-activated slag with calcined oyster shell powder as an activator, considerable dissolution of calcium oxide increased the heat of hydration at an early age.
2) The amount of calcined oyster shell powder added had a considerable impact on strength development in the one-part alkali-activated slag. The dosage of 5% calcined oyster shell powder improved the compressive strength, while the specimen seeded with more than 10% of calcined oyster shell powder showed negative effects of this level on strength development at a later age.
3) TG data up to 200 °C showed that higher dosages of calcined oyster shell powder could produce more C-S-H. However, this is not the primary cause of strength development in one-part alkali-activated slag. Factors such as porosity govern at higher magnitudes, thus determining the development of strength in the present study.
4) A low dosage of calcined oyster shell powder contributed to pore-size refinement, resulting in higher compressive strength values.
5) In conclusion, calcined oyster shell powder can potentially be applied as an environmentally friendly, non-corrosive and non-viscous activator during the production of alkali-activated materials. Moreover, the addition of calcined oyster shell powder as an activator to produce one-part alkali-activated slag can provide a sustainable outlet to recycle and reuse oyster shell waste to develop green and eco-friendly building materials.

CRediT authorship contribution statement

Beomjoo Yang: Conceptualization, Methodology, Resources, Investigation, Writing - review & editing. **Jeong Gook Jang:** Conceptualization, Funding acquisition, Methodology, Investigation, Supervision, Writing - original draft, Writing - review & editing.

Declaration of Competing Interest

The authors declare that they have no known competing financial interests or personal relationships that could have appeared to influence the work reported in this paper.

Acknowledgements

This work was supported by the National Research Foundation of Korea (NRF) grant funded by the Korea government (MSIT) (No. 2018R1C1B6002093). The authors are grateful to Mr. Ali Naqi for the cooperation in the test involved in this study.

References

[1] S.A. Miller, V.M. John, S.A. Pacca, A. Horvath, Carbon dioxide reduction potential in the global cement industry by 2050, Cem. Concr. Res. 114 (2018) 115–124.
[2] K.L. Scrivener, V.M. John, E.M. Gartner, Eco-efficient cements: potential economically viable solutions for a low-CO_2 cement-based materials industry, Cem. Concr. Res. 114 (2018) 2–26.
[3] J.L. Provis, Alkali-activated materials, Cem. Concr. Res. 114 (2018) 40–48.

[4] P. Mec, J. Boháčová, J. Koňařík, Comparison of selected properties of Portland cement based materials and alkali activated materials based on granulated blast furnace slag, Materials Science Forum, Trans Tech Publ, 2016, pp. 107–113.
[5] D.M. Roy, Alkali-activated cements opportunities and challenges, Cem. Concr. Res. 29 (2) (1999) 249–254.
[6] F. Pacheco-Torgal, J. Castro-Gomes, S. Jalali, Alkali-activated binders: a review: Part 1. Historical background, terminology, reaction mechanisms and hydration products, Constr. Build. Mater. 22 (7) (2008) 1305–1314.
[7] A. Palomo, P. Krivenko, I. Garcia-Lodeiro, E. Kavalerova, O. Maltseva, A. Fernández-Jiménez, A review on alkaline activation: new analytical perspectives, Materiales de Construcción 64 (315) (2014) e022.
[8] I. Lecomte, C. Henrist, M. Liegeois, F. Maseri, A. Rulmont, R. Cloots, (Micro)-structural comparison between geopolymers, alkali-activated slag cement and Portland cement, J. Eur. Ceram. Soc. 26 (16) (2006) 3789–3797.
[9] T. Luukkonen, Z. Abdollahnejad, J. Yliniemi, P. Kinnunen, M. Illikainen, One-part alkali-activated materials: a review, Cem. Concr. Res. 103 (2018) 21–34.
[10] M. Kovtun, E.P. Kearsley, J. Shekhovtsova, Dry powder alkali-activated slag cements, Adv. Cem. Res. 27 (8) (2015) 447–456.
[11] H.A. Gawwad, S.A. El-Aleem, A. Ouda, Preparation and characterization of one-part non-Portland cement, Ceram. Int. 42 (1) (2016) 220–228.
[12] B. Nematollahi, J. Sanjayan, F.U.A. Shaikh, Synthesis of heat and ambient cured one-part geopolymer mixes with different grades of sodium silicate, Ceram. Int. 41 (4) (2015) 5696–5704.
[13] B. Nematollahi, J. Sanjayan, J. Qiu, E.-H. Yang, Micromechanics-based investigation of a sustainable ambient temperature cured one-part strain hardening geopolymer composite, Constr. Build. Mater. 131 (2017) 552–563.
[14] K.-H. Yang, J.-K. Song, Workability loss and compressive strength development of cementless mortars activated by combination of sodium silicate and sodium hydroxide, J. Mater. Civ. Eng. 21 (3) (2009) 119–127.
[15] K.-T. Wang, L.-Q. Du, X.-S. Lv, Y. He, X.-M. Cui, Preparation of drying powder inorganic polymer cement based on alkali-activated slag technology, Powder Technol. 312 (2017) 204–209.
[16] K.-H. Yang, J.-K. Song, J.-S. Lee, Properties of alkali-activated mortar and concrete using lightweight aggregates, Mater. Struct. 43 (3) (2010) 403–416.
[17] Y. Alrefaei, Y.-S. Wang, J.-G. Dai, The effectiveness of different superplasticizers in ambient cured one-part alkali activated pastes, Cem. Concr. Compos. 97 (2019) 166–174.
[18] T. Luukkonen, Z. Abdollahnejad, J. Yliniemi, P. Kinnunen, M. Illikainen, Comparison of alkali and silica sources in one-part alkali-activated blast furnace slag mortar, J. Cleaner Prod. 187 (2018) 171–179.
[19] P. Duxson, J.L. Provis, Designing precursors for geopolymer cements, J. Am. Ceram. Soc. 91 (12) (2008) 3864–3869.
[20] M.S. Kim, Y. Jun, C. Lee, J.E. Oh, Use of CaO as an activator for producing a price-competitive non-cement structural binder using ground granulated blast furnace slag, Cem. Concr. Res. 54 (2013) 208–214.
[21] G.-L. Yoon, B.-T. Kim, B.-O. Kim, S.-H. Han, Chemical–mechanical characteristics of crushed oyster-shell, Waste Manage. 23 (9) (2003) 825–834.
[22] E.-I. Yang, S.-T. Yi, Y.-M. Leem, Effect of oyster shell substituted for fine aggregate on concrete characteristics: Part I. Fundamental properties, Cem. Concr. Res. 35 (11) (2005) 2175–2182.
[23] K.H. Mo, U.J. Alengaram, M.Z. Jumaat, S.C. Lee, W.I. Goh, C.W. Yuen, Recycling of seashell waste in concrete: a review, Constr. Build. Mater. 162 (2018) 751–764.
[24] J.H. Seo, S.M. Park, B.J. Yang, J.G. Jang, Calcined oyster shell powder as an expansive additive in cement mortar, Materials 12 (8) (2019) 1322.
[25] D. Khale, R. Chaudhary, Mechanism of geopolymerization and factors influencing its development: a review, J. Mater. Sci. 42 (3) (2007) 729–746.
[26] P. Duxson, A. Fernández-Jiménez, J.L. Provis, G.C. Lukey, A. Palomo, J.S. van Deventer, Geopolymer technology: the current state of the art, J. Mater. Sci. 42 (9) (2007) 2917–2933.
[27] Z. Sun, X. Lin, P. Liu, D. Wang, A. Vollpracht, M. Oeser, Study of alkali activated slag as alternative pavement binder, Constr. Build. Mater. 186 (2018) 626–634.
[28] M. Najimi, N. Ghafoori, Engineering properties of natural pozzolan/slag based alkali-activated concrete, Constr. Build. Mater. 208 (2019) 46–62.
[29] C. Shi, R.L. Day, A calorimetric study of early hydration of alkali-slag cements, Cem. Concr. Res. 25 (6) (1995) 1333–1346.
[30] I. Richardson, H.F. Taylor, Cement chemistry, ICE Publishing, 2015.
[31] I. Ismail, S.A. Bernal, J.L. Provis, R. San Nicolas, S. Hamdan, J.S. van Deventer, Modification of phase evolution in alkali-activated blast furnace slag by the incorporation of fly ash, Cem. Concr. Compos. 45 (2014) 125–135.
[32] S.M. Park, J.G. Jang, H.K. Lee, Unlocking the role of MgO in the carbonation of alkali-activated slag cement, Inorg. Chem. Front. 5 (7) (2018) 1661–1670.
[33] M. Ben Haha, G. Le Saout, F. Winnefeld, B. Lothenbach, Influence of activator type on hydration kinetics, hydrate assemblage and microstructural development of alkali activated blast-furnace slags, Cem. Concr. Res. 41 (3) (2011) 301–310.
[34] M.B. Haha, B. Lothenbach, G. Le Saout, F. Winnefeld, Influence of slag chemistry on the hydration of alkali-activated blast-furnace slag - Part II: Effect of Al_2O_3, Cem. Concr. Res. 42 (1) (2012) 74–83.
[35] J.E. Oh, P.J.M. Monteiro, S.S. Jun, S. Choi, S.M. Clark, The evolution of strength and crystalline phases for alkali-activated ground blast furnace slag and fly ash-based geopolymers, Cem. Concr. Res. 40 (2) (2010) 189–196.
[36] J.I. Escalante-García, A.F. Fuentes, A. Gorokhovsky, P.E. Fraire-Luna, G. Mendoza-Suarez, Hydration products and reactivity of blast-furnace slag activated by various alkalis, J. Am. Ceram. Soc. 86 (12) (2003) 2148–2153.
[37] S.-D. Wang, K.L. Scrivener, Hydration products of alkali activated slag cement, Cem. Concr. Res. 25 (3) (1995) 561–571.
[38] Y. Wei, W. Yao, X. Xing, M. Wu, Quantitative evaluation of hydrated cement modified by silica fume using QXRD, ^{27}Al MAS NMR, TG-DSC and selective dissolution techniques, Constr. Build. Mater. 36 (2012) 925–932.
[39] K.J.D. MacKenzie, R.H. Meinhold, B.L. Sherriff, Z. Xu, ^{27}Al and ^{25}Mg solid-state magic-angle spinning nuclear magnetic resonance study of hydrotalcite and its thermal decomposition sequence, J. Mater. Chem. 3 (12) (1993) 1263–1269.
[40] P. Mehta, P.J.M. Monteiro, Concrete: Microstructure, Properties, and Materials, McGraw-Hill Education, 2006.
[41] H. El-Didamony, A.A. Amer, H. Abd Ela-ziz, Properties and durability of alkali-activated slag pastes immersed in sea water, Ceramics Int. 38(5) (2012) 3773-3780.
[42] P. Yu, R.J. Kirkpatrick, B. Poe, P.F. McMillan, X. Cong, Structure of calcium silicate hydrate (C-S-H): Near-, Mid-, and Far-infrared spectroscopy, J. Am. Ceram. Soc. 82 (3) (1999) 742–748.
[43] M. Criado, A. Fernández-Jiménez, A. Palomo, Alkali activation of fly ash: effect of the SiO_2/Na_2O ratio: Part I: FTIR study, Microporous Mesoporous Mater. 106 (1) (2007) 180–191.
[44] M.Y.A. Mollah, F. Lu, D.L. Cocke, An X-ray diffraction (XRD) and Fourier transform infrared spectroscopic (FT-IR) characterization of the speciation of arsenic (V) in Portland cement type-V, Sci. Total Environ. 224 (1) (1998) 57–68.